Supplemental Data

Metabolite Profiling Identifies Anandamide as a Biomarker of Nonalcoholic Steatohepatitis

W. Taylor Kimberly, MD, PhD,[1] John O'Sullivan, MD, PhD,[2] Anjali K. Nath, PhD,[3] Michelle Keyes, PhD,[4] Xu Shi, PhD,[2] Martin G. Larson, SD,[4,5] Qiong Yang, PhD,[4,5] Michelle T. Long, MD,[4,6] Ramachandran Vasan, MD,[4] Randall T. Peterson, PhD,[3] Thomas J. Wang, MD,[7] Kathleen E. Corey, MD, MPH, MMSc[8] and Robert E. Gerszten, MD[2]

1. Center for Human Genetic Research, Department of Neurology, Massachusetts General Hospital, Boston, MA
2. Division of Cardiovascular Medicine, Beth Israel Deaconess Hospital, Boston, MA
3. Division of Cardiology, Department of Medicine, Massachusetts General Hospital, Boston, MA
4. Framingham Heart Study of the National Heart, Lung, and Blood Institute and Boston University School of Medicine, Framingham, MA
5. Biostatistics Department, Boston University School of Public Health, Boston, MA
6. Section of Gastroenterology, Department of Medicine, Boston University School of Medicine, Boston, MA
7. Division of Cardiovascular Medicine, Department of Medicine, Vanderbilt University, Nashville, TN
8. Division of Gastroenterology, Department of Medicine, Massachusetts General Hospital, Boston, MA

Correspondence:
Robert E. Gerszten, MD
Division of Cardiovascular Medicine
Beth Israel Deaconess Medical Center
330 Brookline Ave
Boston, MA 02115
Email: rgerszte@bidmc.harvard.edu

Supplemental Methods and Results

Analyte selection

In order to develop a multifunctional, high throughput method for human plasma that included sentinel analytes across important metabolic pathways, we first identified 273 metabolites available in purity across major domains of metabolism in the KEGG database. Analytes included central carbohydrates, organic acids, bile acids, sterols, glycans, nucleotides, vitamins, and amino acids. Next, we constrained the design based on the following principles: 1) compatibility with a one-step pre-analytical sample preparation, 2) a rapid LC gradient with sufficient separation of metabolites to allow for multiple reaction monitoring, 3) stable retention times and column life over repeated injections, and 4) optimization of mass spectrometer settings to enhance detection of lower abundance negatively charged metabolites. The conceptual workflow of the LC-MS/MS method is depicted in Supplemental Figure 1. Each metabolite was individually tuned on the platform. The example of 2-aminoadipic acid (2-AAA) demonstrates the identity and separation from isobaric contaminants (Supplemental Fig. 1B). Detection of the endogenous metabolite in plasma was compared to exogenous compound in a pure preparation and exogenous compound spiked into plasma to confirm identity. The expected peak was further identified by examining fragmentation patterns and comparing to pure exogenous compound.

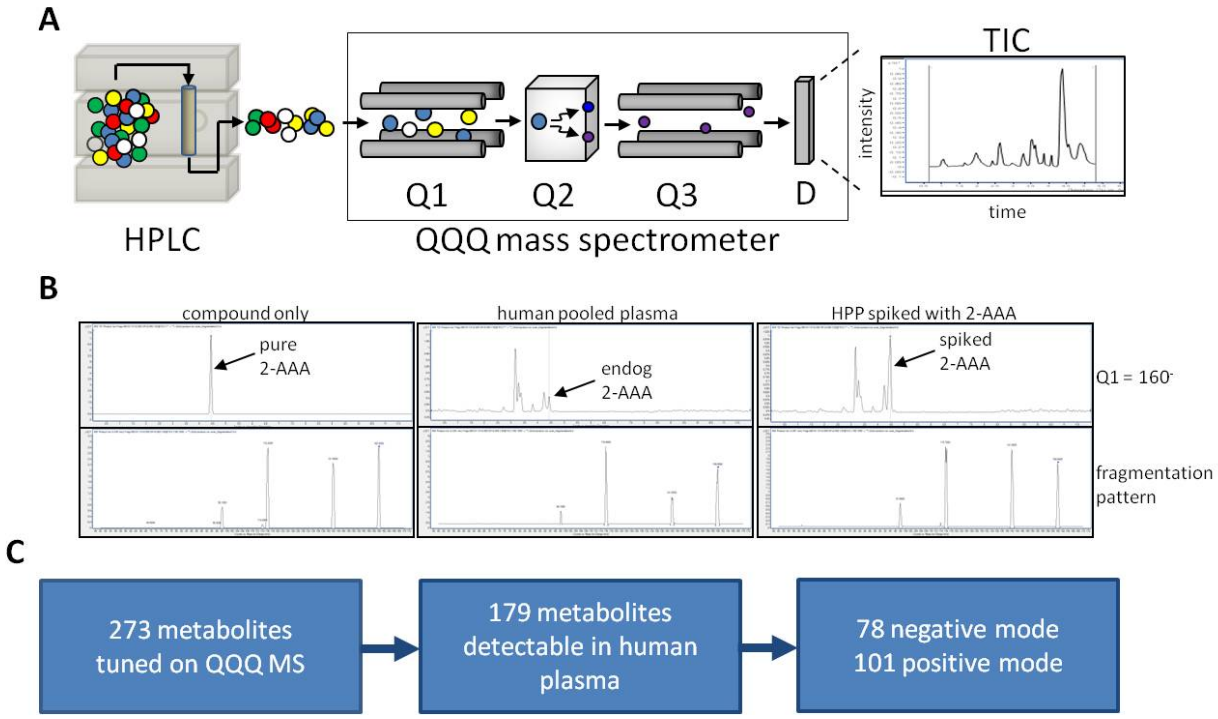

Supplemental Figure 1. Conceptual workflow for metabolite profiling. A) Following precipitation of protein, the complex matrix is first separated using Amide chromatography followed by tandem mass spectrometry to identify each metabolite. **B)** The process for compound identification first involves tuning the instrument to purified compound (left panels). Human pooled plasma is then monitored using the optimized settings (middle panel). Isobaric contaminants demonstrate different retention times and peak identity is further confirmed by comparing fragmentation patterns with the pure compound. Finally, spiked compound is added to the pooled plasma to confirm proper retention time. **C)** Overview of the number of initial compounds tuned on the platform, the number that were detectable in human plasma (middle panel) and the number based on ionization polarity.

Platform settings influence sensitivity in a compound-specific manner

We assessed for analytical parameters that affect sensitivity and reproducibility. We focused on sensitivity first, to maximize the number of monitored analytes detected in a high throughput method. The sensitivity to various metabolite classes was dependent upon source ionization and sample preparation conditions, which influenced detection in a compound-specific manner (see Supplemental Figure 2). For example, altering the desolvation rate by increasing source gas temperatures improved the sensitivity for many compound classes but particularly for nucleotides, high energy phosphates and bile acids (Supplemental Figure 2A). Other source settings related to the electrospray pressure and nozzle voltage demonstrated a trade-off in sensitivity for different metabolite classes (Supplemental Figure 2B). Similarly, the sample preparation solvents influenced both the sensitivity and the ability to detect selected compounds, with acetonitrile:methanol preserving the maximum detection of metabolites with the highest sensitivity (Supplemental Figure 2C). Of 273 compounds evaluated, the final method yielded 179 metabolites that were reproducibly detected in human plasma.

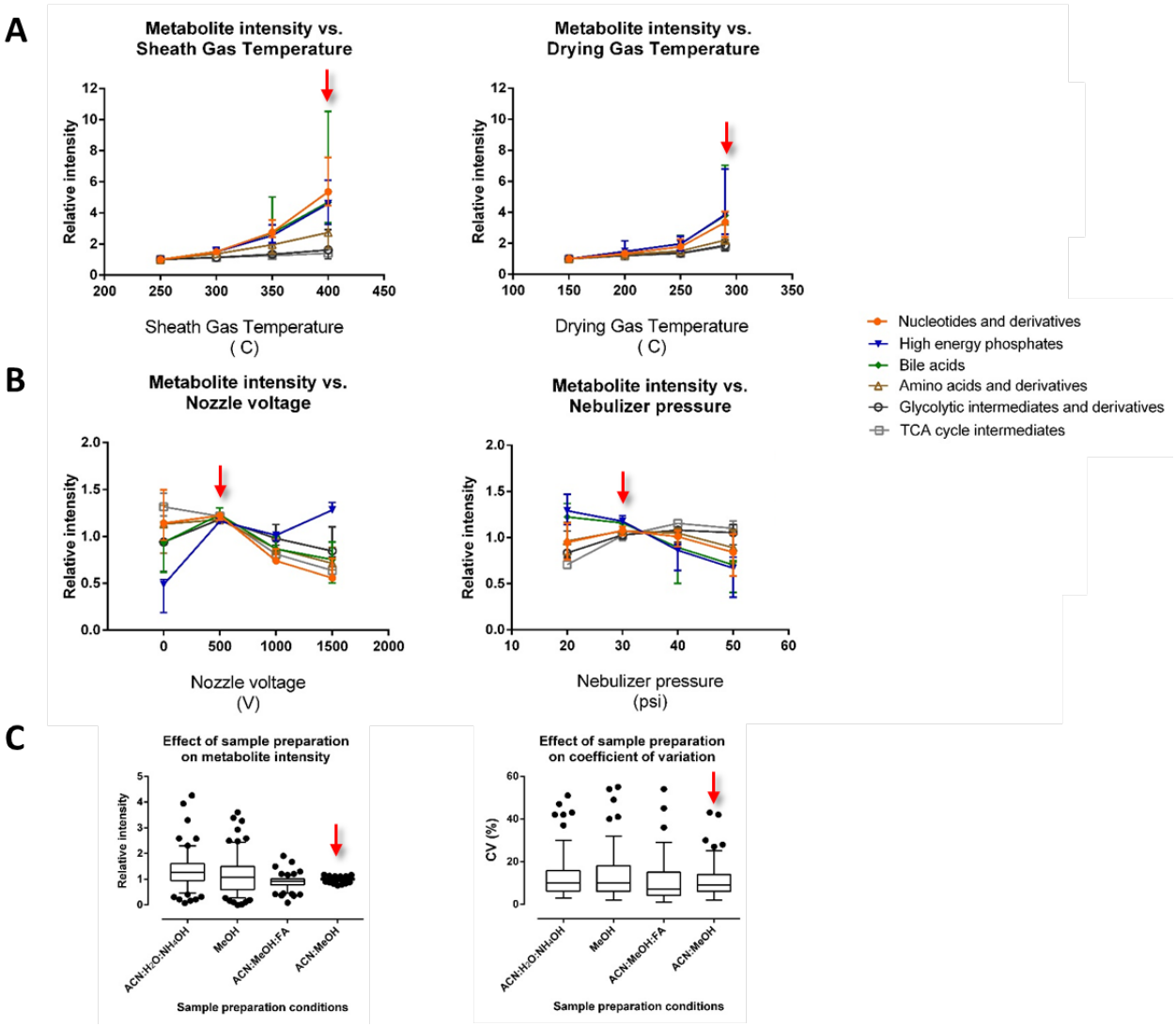

Supplemental Figure 2. Sensitivity for detection varies in a compound-specific manner. A) Ionization source settings that impact the desolvation rate, including the sheath and drying gas temperatures affect sensitivity that varies by compound class. The arrow marks the final setting used for subsequent analysis. **B)** Source voltage and nebulizer pressures demonstrate a trade-off in the detection of compound classes, with the optimal setting highlighted by the red arrows. **C)** Sample preparation solvents altered the sensitivity for detection of compounds, and to a lesser extent, the coefficient of variation (CV).

Analysis of retention time, normalization procedures and reproducibility

We conducted a test run composed of 700 sample injections to evaluate retention time (RT) and reproducibility of the normalization procedure. Evaluating the RTs for all analytes demonstrated that temporal drift remained within a ~5 second window throughout the run (Supplemental Figure 3A). In order to evaluate analytical reproducibility, we first corrected for the effect of ionization suppression, a consequence of electrospray ionization related to the accumulation of salts and sample biomass in the ionization source that can lead to sensitivity drift over time (Supplemental Figure 3B).[1] Interspersed pooled plasma reference samples allowed for correction of the anticipated sensitivity drift (Supplemental Figure 3C), resulting in coefficient of variation (CV) of 4.3% to 11.9% for the deuterated internal standards (Supplemental Figure 3D). Measurement variation was also specific to each analyte[2] in the pooled plasma reference samples, with CV ranging from 1.0% to 22.1% (see Supplemental Table 1).

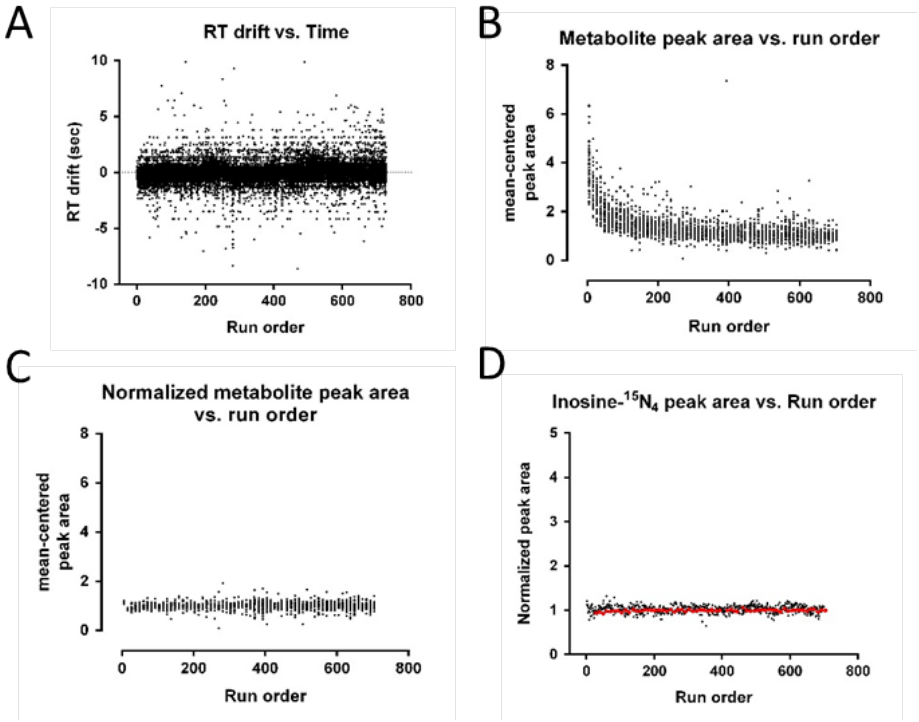

Supplemental Figure 3. Assessment of reproducibility and validation of the pooled plasma normalization procedure. A) The retention time (RT) drift over a 700 sample injection run is plotted for all metabolites on a sample by sample basis. With a multiple reaction monitoring window of 30-60 seconds per metabolite allows for the observed drift in retention time over long runs. **B)** Ionization suppression is evident in negative mode Amide LC-MS/MS, which is related to the accumulation of salts and biomass that occurs with repeated injections. **C)** Normalization on a metabolite-by-metabolite basis corrects sensitivity drift. Data for interspersed human pooled plasma samples are shown. **D)** Deuterated internal standards are included in every sample to visualize and confirm expected sensitivity and normalization. Inosine-$^{15}N_4$ is shown as an example, which had a CV of 5.6% across all injections.

The biological range of values for each metabolite within the experimental samples varied to a greater extent than analytical variation, although some metabolites demonstrated less variation suggestive of tighter regulation (e.g., citrulline, Supplemental Figure 4A). Other analytes demonstrated wider variation in concentration in the experimental samples (e.g., the ketone body 3-hydroxybutyrate, Supplemental Figure 4B), suggestive of a greater tolerance in concentration range within the bloodstream. For each metabolite, the relationship between the analytical and biological variation (Supplemental Figure 4C) was determined by the interaction between platform analytical performance and the biological concentration range in the plasma. For some compound classes such as the ketone bodies and bile acids, there was approximately a five-fold greater biological to analytical variation whereas the TCA cycle organic acids demonstrated less dynamic range (Supplemental Figure 4C, red versus green dots, respectively).

To assess suitability for population based studies, we developed clinical sample size estimates which varied depending on the analytical variation for each metabolite and the biological variation of the analyte within the experimental samples (i.e., the difference between the means). Generalizing this concept, we modeled this relationship based on sample size for group size *N*, the difference between the means (as a percentage) and the CV at 80% power, using a Bonferroni-corrected type I error rate for 179 tests, $\alpha=2.79\times10^{-4}$.[3] Sample size calculations were modeled for different coefficient of variation thresholds based on the equation:

$$n = \frac{(z_{1-\alpha/2} + z_{1-\beta})^2 \, CV^2 \, (f^2+1)}{(f-1)^2}$$

where n is the number of observations per group, z is the z score for the standard normal distribution, f is the ratio of the means between each group, Type I error is set at $\alpha=2.79\times10^{-4}$ and the power is set at $1-\beta=0.80$.[3]

Given the observed analytical variability up to 22.1%, a cohort of 1,000 subjects would have 80% power to detect a difference of 8% or less for all metabolites included in the platform (Supplemental Figure 4D), which corresponds to a magnitude commonly seen in metabolite profiling studies.[4-7]

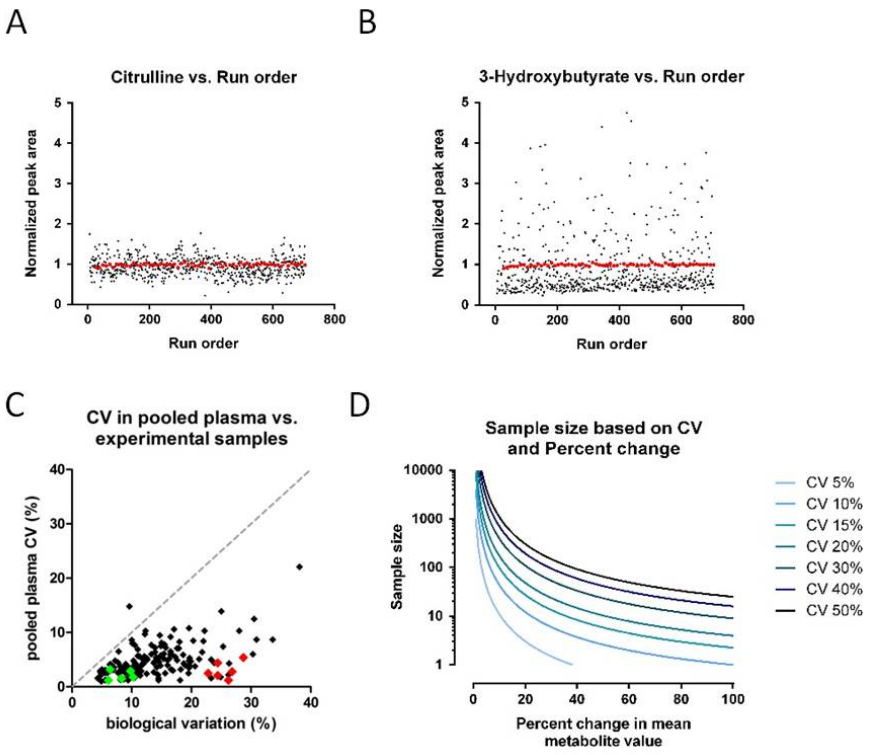

Supplemental Figure 4. Both analytical and biological factors are analyte specific and determine the power in a given sample size. **A)** On a metabolite-by-metabolite basis, the reproducibility of detection was monitored throughout the analytical run by interspersing human pooled plasma replicates (red dots). The experimental samples (black dots) are representative of the biological variability of the metabolite. Citrulline demonstrated less biological variability relative to **B)** the ketone body, 3-hydroxybutyrate. **C)** Summary of the analytical coefficient of variation (CV) in pooled plasma replicates relative to the biological variation of the experimental samples. As illustrative examples, ketone bodies and bile acids (red dots) demonstrated greater biological variation than tricarboxylic organic acids (green dots). **D)** Sample size estimates are modeled based on a given analytical CV (each line represents a different CV threshold), the percentage difference in values between cases and controls. For these models, 80% power and a Bonferroni-corrected type I error rate for 179 tests, $\alpha=2.79\times10^{-4}$ was used.

Peak validation of anandamide

Each metabolite was individually tuned on the platform. Detection of the endogenous metabolite in plasma was compared to exogenous compound in a pure preparation and exogenous compound spiked into plasma to confirm identity. Supplemental Figure 5 shows the chromatograms from anandamide (AEA), which demonstrate the unambiguous identity of pure exogenous anandamide injected onto the LC-MS system (Supplemental Fig. 5A), which also corresponds to the same peak when exogenous AEA was spiked into human plasma (Supplemental Fig. 5B). The endogenous AEA in human plasma (Supplemental Fig. 5C) was detected and showed no isobaric contaminants. Both high and low endogenous AEA (Supplemental Fig. 5D) from experimental samples are shown.

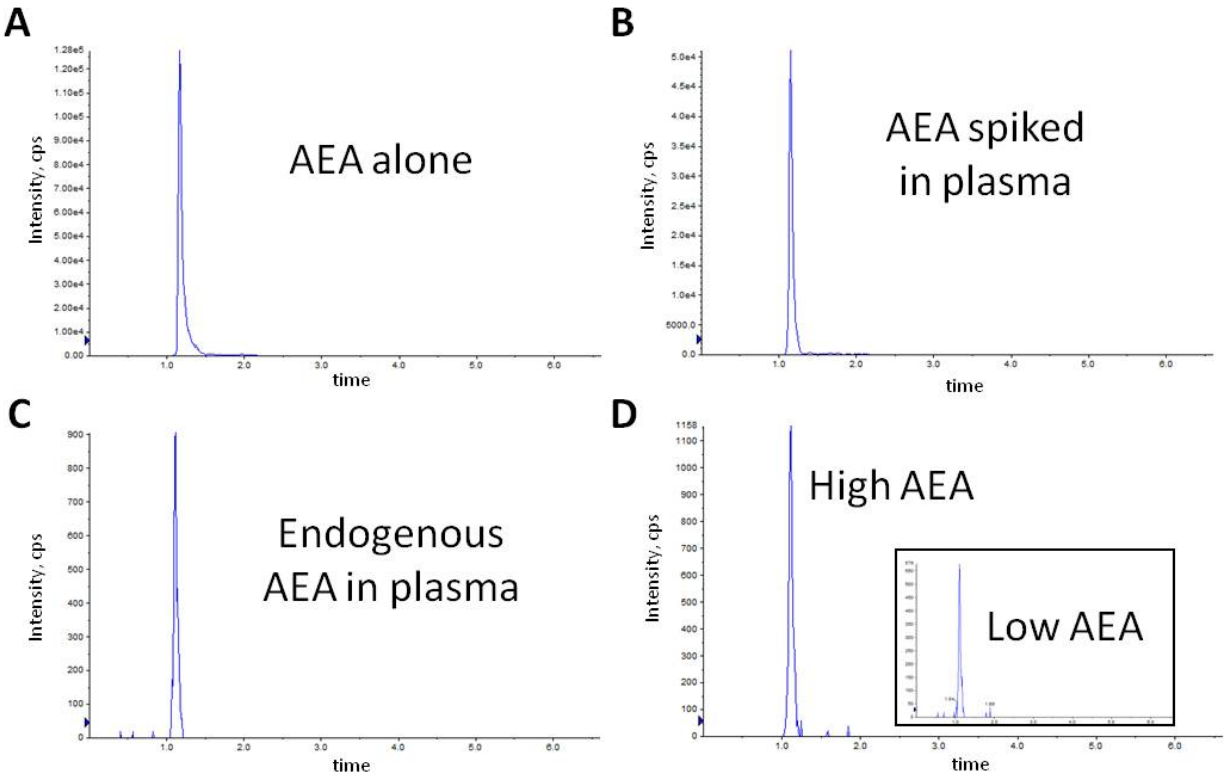

Supplemental Figure 5. Validation and peak identity of anandamide in the Amide LC-MS method. A) Exogenous anandamide (AEA) was injected into the LC-MS using the Amide method. The AEA peak, with MRM transitions of Q1: 348, Q3: 62.3, is shown in panel A. **B)** Anandamide was also spiked into normal volunteer human plasma, and the same peak was

identified. **C)** The endogenous level of anandamide was detected at the same retention time, and no contaminating peaks were detected elsewhere in the run with same MRM settings. **D)** Two examples of experimental samples from the Framingham Heart Study Generation 3 cohort, with high endogenous anandamide (larger panel) and low endogenous anandamide (inset). Note that the low AEA chromatogram is scaled to match the high AEA peak intensity so that the peak and area of each peak can be directly compared.

Anandamide concentration in plasma

To estimate the absolute concentration of anandamide in plasma, exogenous deuterated anandamide-d_4 was spiked into human pooled plasma across a broad concentration range. Supplemental Figure 6 shows the wide linear range (right hand panel) as well as the range that corresponds to the concentration of endogenous anandamide (left hand panel). The calculated concentration in human pooled plasma was 106 ± 5.7 pg/ml.

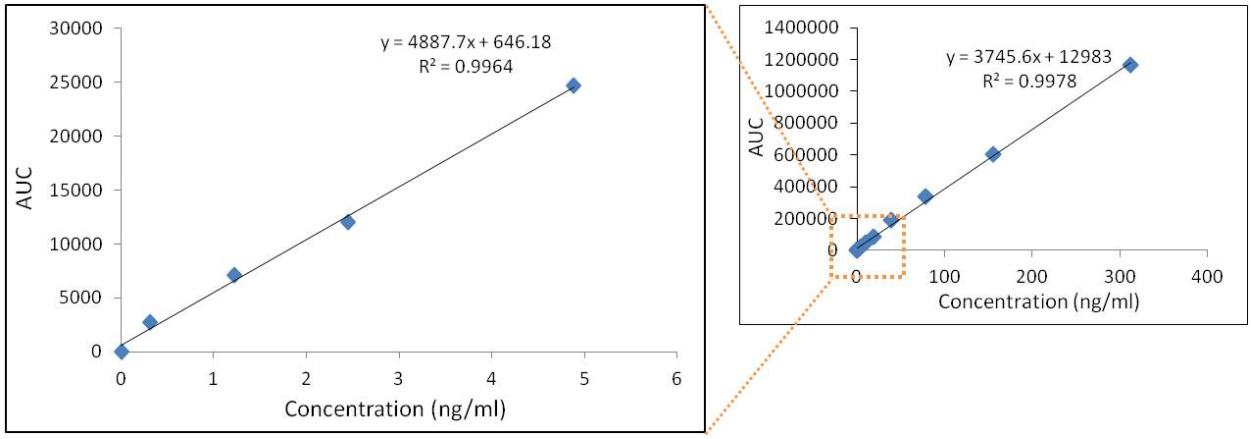

Supplemental Figure 6. Standard curve demonstrating the range of detection of anandamide-d_4 in human plasma. A) Isotopically labeled anandamide-d_4, was spiked into human plasma at the indicated concentrations and analyzed using the LC-MS amide protocol. The lefthand panel is an inset that corresponds to the organge dotted rectangle on the righthand panel. Based on the standard curve, endogenous anandamide in normal volunteer plasma was measured at 106 ± 5.7 pg/ml, which is consistent with published concentration ranges.

***D. rerio* experiments**

Zebrafish (Ekkwill strain) were maintained and embryos were obtained according to standard fish husbandry protocols in accordance with the Massachusetts General Hospital Institutional Animal Care and Use Committee. All compounds were purchased from Sigma-Aldrich. Compounds were incubated for the indicated times, and the concentration indicates the level in the water. The corresponding level within the fish varies based on absorption through the skin, metabolism and excretion. However, the level of anandamide obtained within the zebrafish, as measured by mass spectrometry, exceeded the endogenous level in order to demonstrate an effect of administration even if greater than physiological normal levels. Post treatment, viability of the zebrafish larvae was assessed by observing heart rate and sedation was assessed by the touch response reflex. Glucose concentration was measured using Amplex Red Glucose Assay Kit (Invitrogen) and converted to uM concentration using a standard curve, according to the manufacturer's instructions. Product formation was determined by reading fluorescence emission at 595nm. Lipid deposition was assessed using Oil Red O staining. Zebrafish were fixed in 4% paraformaldehyde, stained with 0.3% Oil Red O in propylene glycol, washed with propylene glycol and imaged in 80% glycerol. Triglycerides were measured in whole zebrafish larvae by homogenizing 20 fish in 50 µl of water. The lysate was centrifuged at 6000 RPM for 10 minutes at 4°C and the supernatant was used to assess triglyceride levels using the Cayman Chemical kit according to the manufacturer's instructions.

Accumulation of AEA within the fish embryos was confirmed by comparison to anandamide-d_4 internal standard two hours after addition of 30 µM AEA to the water (Figure 7A). To determine the effect of acute administration of AEA on glucose homeostasis, zebrafish larvae 6 days post fertilization (dpf) were supplemented with AEA. One hour post

administration, larvae displayed elevated glucose levels (10,067±345 RFU vs 7,653±312 RFU, p=0.0001; Figure 7B, left panel). At the highest concentration (30 μM AEA), there was a 32% elevation in glucose at 1 hour, a 43% elevation at 2 hours ($p=6.46 \times 10^{-5}$) and a 33% increase at 4 hours (9,917±475 RFU vs 13,194±1,129 RFU, p=0.0003). Co-administration with the cannabinoid receptor inhibitor rimonabant ameliorated the AEA-induced elevation in glucose, underscoring the specificity of the observations (Figure 7B, right panel).

In zebrafish, adipocytes do not develop until 12 dpf. However, younger zebrafish larvae have a characteristic pattern of lipid deposition which can be visualized with the fat soluble dye, Oil Red O. Typically, unfed larvae display low levels of neutral triglycerides and lipids in the central nervous system and yolk sac. The baseline level of lipid deposition was represented by 6 dpf control larvae (Figure 7C, top left panel). In contrast, larvae incubated with AEA displayed an increased amount of Oil Red O staining in several organ regions that was inhibited by co-administration of rimonabant (Fig 7C), particularly the liver which demonstrated a dose-dependent increase in staining (Figure 7D, boxes). Concordant with that observation, AEA induced a 39% increase in triglyceride levels in zebrafish larvae (13.3±0.01 mg/dl vs. 18.5±0.01 mg/dl, p=0.001; Figure 7E). The effect of AEA administration was not exclusive to the liver. Additional organ areas were also detected with Oil Red O, including the brain and vascular system (Figure 7F). Within the brain, Oil Red O staining was prominent in the diencephalon (Figure 7F, arrowheads) and the optic tectum. Within the vascular system of fish treated with AEA, the dorsal aorta, axial vein and intrasegmental blood vessels (Figure 7F, arrows) were enriched with lipid deposits compared to the absence of vascular lipid deposits in vehicle-treated control larvae.

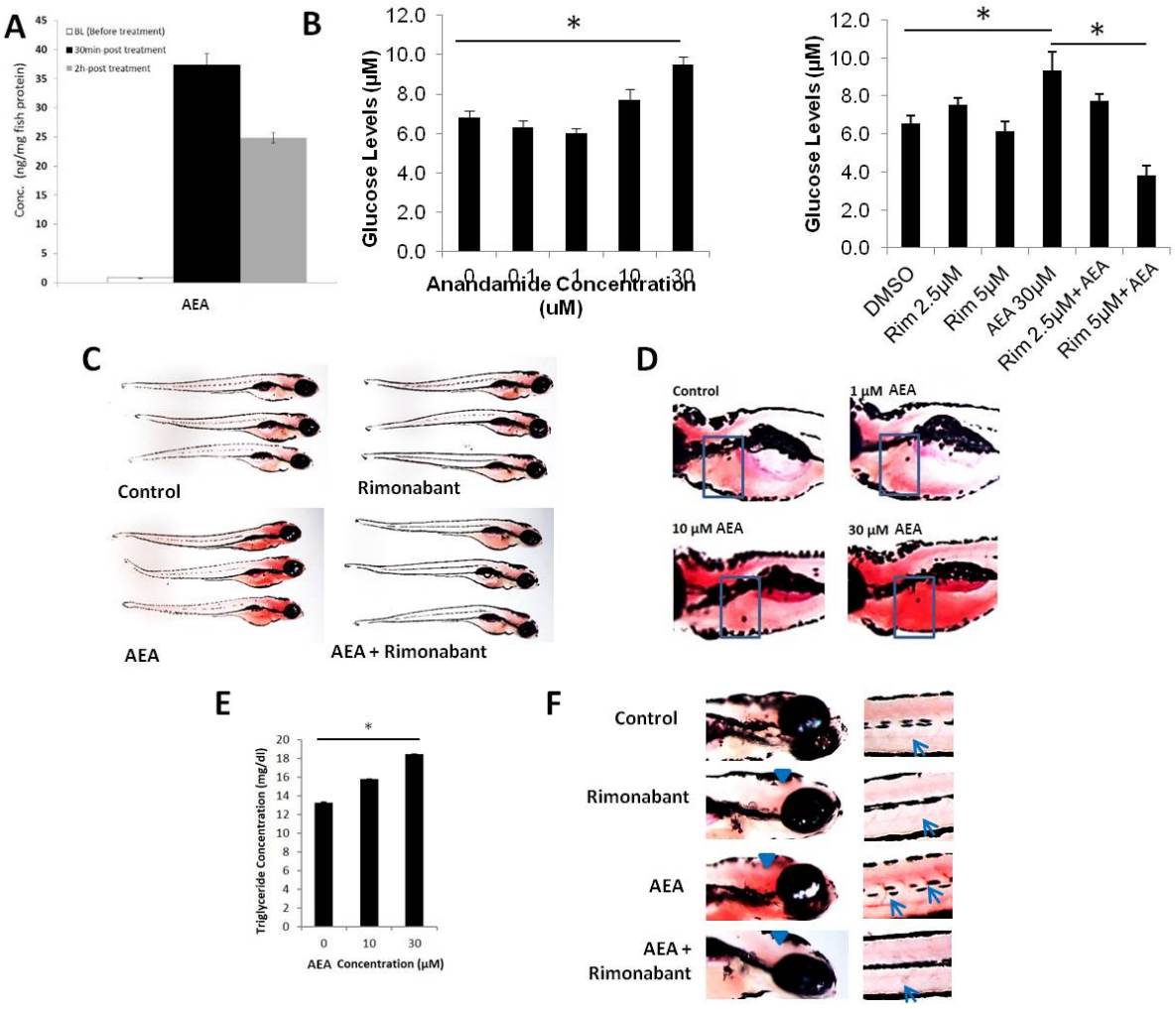

Supplemental Figure 7. Exogenous anandamide administration in zebrafish alters glucose levels and lipid accumulation. A) The concentration of AEA achieved within the fish was measured by comparing to deuterated anandamide-d_4, normalized to total fish protein. AEA, anandamide. **B)** Glucose levels were measured in 6 dpf larvae 4 hours post treatment with the increasing concentration of AEA in the water. Glucose was also measured in the presence of rimonabant, a cannabinoid receptor inhibitor. *, $p<0.001$; Glucose measurements provided in uM concentration; AEA, anandamide; Rim, rimonabant; data are mean±SEM. **C)** 6 dpf larvae stained with Oil Red O viewed laterally. **D)** Magnified views of the zebrafish, with the liver visualized by turning the fish to the left side. The location of the liver is shown by the blue box. **E)** Triglyceride concentration was measured in whole zebrafish larvae after treatment with increasing doses of AEA. *, $p=0.001$. **F)** Additional areas of AEA-dependent lipid staining included the brain (arrowheads) and the intersegmental vessels (arrows).

References

1. Annesley, T.M. Ion suppression in mass spectrometry. *Clinical chemistry* **49**, 1041-1044 (2003).
2. Dunn, W.B.*, et al.* Procedures for large-scale metabolic profiling of serum and plasma using gas chromatography and liquid chromatography coupled to mass spectrometry. *Nature protocols* **6**, 1060-1083 (2011).
3. Van Belle, G. & Martin, D.C. Sample size as a function of coefficient of variation and ratio of means. *The American Statistician* **47**, 165-167 (1993).
4. Wang, T.J.*, et al.* Metabolite profiles and the risk of developing diabetes. *Nat Med* **17**, 448-453 (2011).
5. Rhee, E.P.*, et al.* Lipid profiling identifies a triacylglycerol signature of insulin resistance and improves diabetes prediction in humans. *J Clin Invest* **121**, 1402-1411 (2011).
6. Rhee, E.P.*, et al.* A genome-wide association study of the human metabolome in a community-based cohort. *Cell Metab* **18**, 130-143 (2013).
7. Kimberly, W.T., Wang, Y., Pham, L., Furie, K.L. & Gerszten, R.E. Metabolite profiling identifies a branched chain amino acid signature in acute cardioembolic stroke. *Stroke; a journal of cerebral circulation* **44**, 1389-1395 (2013).